Manuscript prepared for The Cryosphere
with version 2015/11/06 7.99 Copernicus papers of the LaTeX class copernicus.cls.
Date: 28 June 2016

Critical investigation of calculation methods for the elastic velocities in anisotropic ice polycrystals

A. Maurel[1], J.-F. Mercier[2], and M. Montagnat[3]

[1] Institut Langevin, CNRS, ESPCI ParisTech, 1 rue Jussieu, 75005 Paris, France
[2]Poems, CNRS, ENSTA ParisTech, INRIA, 828 boulevard des Maréchaux 91762 Palaiseau, France
[3]LGGE, CNRS, Université Grenoble Alpes, 38041 Grenoble, France.

Correspondence to: A. Maurel (agnes.maurel@espci.fr)

Abstract.

Crystallographic texture (or fabric) evolution with depth along ice cores can be evaluated using borehole sonic logging measurements. These measurements provide the velocities of elastic waves that depend on the ice polycrystal anisotropy, and can further be related to the ice texture. To do so, elastic velocities need to be inverted from a modeling approach that relate elastic velocities to ice texture. So far, two different approaches can be found. A classical model is based on the effective medium theory; the velocities are derived from elastic wave propagation in a homogeneous medium characterized by an average elasticity tensor. Alternatively, a velocity averaging approach was used in the glaciology community, that averages the velocities from a given population of single crystals with different orientations.

In this paper, we show that the velocity averaging method is erroneous in the present context. This is demonstrated for the case of waves propagating along the clustering direction of a highly textured polycrystal, characterized crystallographic c-axes oriented along a single maximum (cluster). In this case, two different shear wave velocities are obtained while a unique velocity is theoretically expected. While making use of this velocity averaging method, reference work by Bennett (1968) does not end with such an unphysical result. We show that this is due to the use of erroneous expressions for the shear wave velocities in a single crystal, as the starting point of the averaging process.

Because of the weak elastic anisotropy of ice single crystal, the inversion of the measured velocities requires accurate modeling approaches. We demonstrate here that the inversion method based on the effective medium theory provides physically based results and should therefore be favored.

1 Introduction

Wave propagation in glaciology is mostly regarded in the context of seismic waves, see *e.g. Kohnen* (1974), *Blankenship et al.* (1987). More recently, a new interest has emerged with the idea of using in situ wave velocity measurements along ice boreholes in order to evaluate the texture (fabric) anisotropy and its evolution with depth along deep ice cores. Such measurements are based on sonic

logging that evaluates the travel time of elastic waves propagating in the ice over a short distance (typically few meters). A classical sonic logger was recently used during a measurement campain at EPICA Dome C (East Antarctica) (*Gusmeroli et al.*, 2012) and revealed the sensitivity of the elastic velocities on the degree of anisotropy of ice polycrystals characterized by a cluster-type texture (with c-axis orientations clustered around the vertical direction), that varies with depth. The measured velocity changes are small, and the inversion procedure to access to the texture estimation is dependent on the level of uncertainties in the measurements. Strong motivation therefore arises for the development of accurate modeling for the inversion of the elastic velocities into the local ice anisotropy.

In a previous paper (*Maurel et al.*, 2015) we applied a classical model for wave propagation in polycrystals to some of the most specific textures that are found in ice recovered from deep ice cores, namely clusters with a vertical transverse isotropy (VTI), as described before, and girdles with a horizontal transverse isotropy (HTI). The latter corresponds to crystallographic c-axes mostly aligned in a vertical plan, and that form in situations where a horizontal tension dominates the stress field. The model used relies on the definition of an *effective medium* characterized by an averaged elasticity tensor defined at the scale of many grains (the polycrystal). (*Maurel et al.*, 2015) presented a comparison with Bennett's predictions (*Bennett*, 1968), which are based on the velocity averaging method, and illustrated the weak differences in the velocities predicted by the two models for VTI clustered textures. Contrary to the effective medium theory, the velocity averaging method does not rely on a rigorous mathematical formalism. Thus, beyond the relative agreement observed for clustered textures, the correctness of the velocity averaging method can be questioned.

This is the goal of the present paper. We will show that the velocity averaging method is based on an erroneous fundamental assumption. To do so, we perform a demonstration for the cases of cluster and girdle ice textures with VTI. It is found that a wave propagating along the vertical axis is associated with two different shear velocities, which is unphysical since the polarizations of the shear waves are in the plane of isotropy. In *Bennett* (1968) a unique expression of the shear velocity was obtained, starting with modified expressions of the two shear wave velocities in ice single crystals. The modification consisted in attributing symmetrical weights to both velocities in order to get the same value after the velocity averaging. It resulted in a velocity value close to the harmonic mean of the two unphysical shear velocities derived from the direct use of the velocity averaging method.

Considering the low elastic anisotropy of the ice single crystal, the accuracy of the inversion procedure from the measured velocities to ice texture is essential. In particular, a model relying on a rigorous mathematical formalism is required, in order to describe the case of complex textures, beyond the simple case of VTI clusters. With regard to this requirement, we will show that the model based on the effective medium theory appears more reliable.

2 Classical results on polycrystal effective anisotropy and wave propagation in anisotropic media

In this section, we recall classical results (i) on the propagation of elastic waves in a crystal or in a polycrystal characterized by a uniform elasticity tensor and (ii) on the elasticity tensor of polycrystals, considered at the scale of many grains as an equivalent "single" crystal. This allows to introduce the notations that will be used in the sequel, and to clarify in a self consistent way some properties that will be needed.

2.1 Wave propagation in a uniform anisotropic medium – The Christoffel equation

In the following, we denote $\mathbf{x} = (x_1, x_2, x_3)$ the spatial coordinates, $\mathbf{u}(\mathbf{x}) = (u_1(\mathbf{x}), u_2(\mathbf{x}), u_3(\mathbf{x}))$ the elastic displacement vector, ρ the constant mass density and c_{abcd} the elasticity tensor being uniform in space. The case of a uniform c_{abcd} corresponds either to a single crystal or to a polycrystal thought as an effective medium and in this latter case, c_{abcd} characterizes the texture of the polycrystal. The propagation of monochromatic waves of frequency ω is described by the wave equation

$$\rho\omega^2 u_a(\mathbf{x}) + c_{abcd}\frac{\partial^2}{\partial x_b \partial x_c} u_d(\mathbf{x}) = 0, \tag{1}$$

with $a = 1, 2, 3$ and and where repeated indices mean summation (Einstein convention). Denoting $\mathbf{k} = k\mathbf{n}$ the wavevector (k is the wavenumber) with $\mathbf{n} = (n_1, n_2, n_3)$ the unitary vector along $\mathbf{k}$, the elastic displacement reads $u_a(\mathbf{x}) = U_a e^{i\mathbf{k}.\mathbf{x}}$ leading to $\rho\omega^2 U_a - k^2 c_{abcd} n_b n_c U_d = 0$ for $a = 1, 2, 3$. This system of equations admits non zero solutions for (U_1, U_2, U_3) if the determinant of the matrix $\rho\omega^2\delta_{ad} - k^2 c_{abcd} n_b n_c$ vanishes (δ_{ab} is the Kronecker symbol). One gets the dispersion relation that links k and ω; equivalently, introducing the phase velocity $V = \omega/k$, we get the classical form of the Christoffel equation

$$\text{Det}\left[\rho V^2 \delta_{ad} - c_{abcd} n_b n_c\right] = 0. \tag{2}$$

The Christoffel equation admits in general three solutions $V = V_P, V_{SH}, V_{SV}$ that are the elastic velocities of the longitudinal wave and the two transverse waves (P, SH and SV stand for pressure wave, shear horizontal and shear vertical waves). It is important to stress at this point that the three values of V^2 being the eigenvalues of the matrix $c_{abcd} n_b n_c/\rho$, they do not depend on the particular frame $(\mathbf{e}_1, \mathbf{e}_2, \mathbf{e}_3)$ used to express c_{abcd}. On the contrary, the eigenvectors (U_1, U_2, U_3) associated to the eigenvalues obviously depend on the frame where they are expressed.

2.2 Elasticity tensor of the polycrystal resulting from anisotropy from grain to grain

In the previous section, we have considered the uniform elasticity tensor of a polycrystal. This elasticity tensor is derived from the characteristics of the grains which compose the polycrystal. For ice,

each grain is composed of the same single crystal with hexagonal symmetry being characterized by its elasticity tensor c^0_{ijkl}, written in terms of C^0_{IJ} in the Voigt's notation (*Voigt*, 1928). The superscript 0 refers to an elasticity tensor expressed in the frame of its principal axes, with the c-axis being oriented along $\mathbf{e}_3$, hereafter referred as the vertical axis. The Voigt's matrix C^0 (with elements C^0_{IJ}, $I = 1,\dots 6$ and $J = 1,\dots 6$) reads

$$\mathsf{C}^0 = \begin{pmatrix} A & A-2N & F & 0 & 0 & 0 \\ A-2N & A & F & 0 & 0 & 0 \\ F & F & C & 0 & 0 & 0 \\ 0 & 0 & 0 & L & 0 & 0 \\ 0 & 0 & 0 & 0 & L & 0 \\ 0 & 0 & 0 & 0 & 0 & N \end{pmatrix}, \tag{3}$$

with the standard notations

$$\begin{cases} c_{ijk\ell} \to C_{IJ}, \\ \text{for} \quad (i,j) \to I, \quad (k,l) \to J, \\ \text{and} \quad (1,1) \to 1, (2,2) \to 2, (3,3) \to 3, \\ \qquad (3,2), (2,3) \to 4, (3,1), (1,3) \to 5, (1,2), (2,1) \to 6. \end{cases} \tag{4}$$

For an arbitrary direction of the c-axis (Fig. 1)

$$\hat{\mathbf{c}} = (\sin\theta\cos\varphi, \sin\theta\sin\varphi, \cos\theta), \tag{5}$$

the elasticity tensor c_{abcd} is deduced from c^0_{ijkl} following

$$c_{abcd} = R_{ia} R_{jb} R_{kc} R_{ld} c^0_{ijk\ell}, \tag{6}$$

with R the rotation matrix (with elements R_{ij})

$$\mathsf{R} \equiv \begin{pmatrix} \cos\theta\cos\varphi & \cos\theta\sin\varphi & -\sin\theta \\ -\sin\varphi & \cos\varphi & 0 \\ \sin\theta\cos\varphi & \sin\theta\sin\varphi & \cos\theta \end{pmatrix}. \tag{7}$$

c_{abcd} depends on (θ, φ) which are the usual angles in spherical coordinates.

The anisotropy at the macroscopic scale (at the scale of many grains) results from the many (or few) possible orientations of the c-axis in each grain. This distribution of c-axes is defined by a probability distribution function $p(\theta, \varphi)$ satisfying

$$\int \mathrm{d}\Omega \, p(\theta,\varphi) = 1, \quad \text{with } \mathrm{d}\Omega \, = \sin\theta \, \mathrm{d}\theta\mathrm{d}\varphi. \tag{8}$$

The elasticity tensor c^{eff}_{ijkl} and the associated Voigt's matrix C^{eff}_{IJ} of the polycrystal can be calculated by means of the average of the elasticity tensors of the grains following

$$c^{\text{eff}}_{ijkl} = \int \mathrm{d}\Omega \; p(\varphi,\theta) c_{ijkl}, \quad C^{\text{eff}}_{IJ} = \int \mathrm{d}\Omega \; p(\varphi,\theta) C_{IJ}, \tag{9}$$

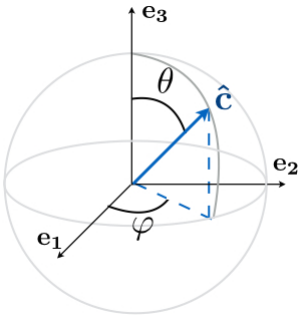

Figure 1. Spherical angles (φ, θ) used for the orientation of the c-axis, ($\hat{\mathbf{c}}$ is an unitary vector).

with the same index convention, Eq. (4), between the elasticity tensor c_{ijkl}^{eff} and the Voigt matrix C_{IJ}^{eff}. For VTI textures, the direction of the axis of anisotropy is given by the effective c-axis, denoted $\hat{\mathbf{c}}^{\text{eff}}$.

For the numerical application, we will use the elastic constants as used in *Bennett* (1968):

$$\text{Ice single crystal} \begin{cases} A = 14.06 \times 10^9 \text{ N.m}^{-2},\ C = 15.24 \times 10^9 \text{ N.m}^{-2},\ L = 3.06 \times 10^9 \text{ N.m}^{-2}, \\ N = 3.455 \times 10^9 \text{ N.m}^{-2},\ F = 5.88 \times 10^9 \text{ N.m}^{-2},\ \rho = 917 \text{ kg/m}^3. \end{cases} \tag{10}$$

3 Elastic wave velocities in the velocity averaging method and velocities of the effective medium for VTI textures

In this section, we compare the elastic velocities obtained from the velocity averaging method, as used in *Bennett* (1968); *Gusmeroli et al.* (2012); *Vélez et al.* (2016), and the elastic velocities obtained from the effective medium theory. The two approaches are as follow

Velocities from the velocity averaging method

First, solve the Christoffel equation for given (θ, φ) :

$$V(\theta,\varphi) = V_P, V_{SV}, V_{SH} \text{ are the roots of } \text{Det}\left[\rho V^2 \delta_{il} - c_{ijkl} n_j n_k\right],$$

Then compute the average of the slowness, from which: $V^{\text{av}} = \left[\int \mathrm{d}\Omega\, p(\theta,\varphi) V^{-1}(\theta,\varphi)\right]^{-1}$.

(11)

Velocities of the effective medium

First, compute the effective elasticity tensor: $c^{\text{eff}}_{ijkl} = \int \mathrm{d}\Omega\, p(\theta,\varphi) c_{ijkl}$,

Then, solve the Christoffel equation:

$$V = V_P^{\text{eff}}, V_{SV}^{\text{eff}}, V_{SH}^{\text{eff}} \text{ are the roots of Det} \left[\rho V^2 \delta_{il} - c^{\text{eff}}_{ijkl} n_j n_k\right]. \quad (12)$$

Below, we report examples of VTI textures for which the velocity averaging method leads to inconsistent results. In such media and for a wave propagating along the vertical direction $\mathbf{e}_3$, the shear displacements are in the plane $(\mathbf{e}_1, \mathbf{e}_2)$, that is in the plane where the response of the polycrystal is isotropic. Thus, there is a unique shear velocity in this particular case ($V_{SV} = V_{SH}$).

Two examples of VTI structures will be presented and the propagation along the vertical direction is considered. The first structure is artificial, with a c-axis associated to a unique $\theta = \theta_0$ value in $[0, \pi/2]$ (and $\varphi \in [0,\ 2\pi]$), but it provides explicit expressions of the velocities in both approaches. It could be seen as a girdle with VTI, (*Azuma and Goto-Azuma*, 1996) with a single zenith angle θ_0, Fig. 2. The second example corresponds to a cone representative of clustered textures measured along ice cores (*Gusmeroli et al.*, 2012; *Diez and al.*, 2015), with $\theta \in [0,\ \theta_0]$ (and $\varphi \in [0,\ 2\pi]$) and is studied numerically, Fig. 3.

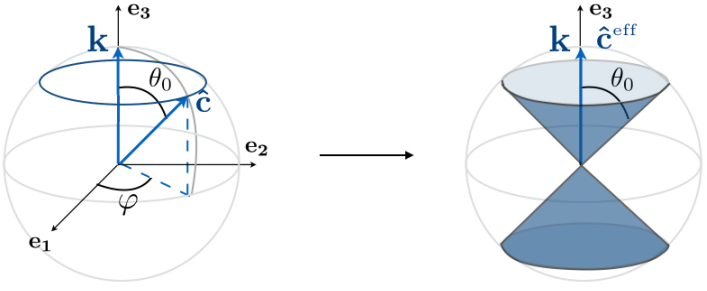

(a) (b)

Figure 2. First configuration of a VTI girdle with a single zenith angle θ_0. (a) shows a typical c-axis $\hat{\mathbf{c}} = (\sin\theta_0\cos\varphi, \sin\theta_0\sin\varphi, \cos\theta_0)$ within one grain, with a constant θ_0, and φ varies randomly from grain to grain. (b) shows the resulting VTI texture of the polycrystal at the macroscopic scale. $\hat{\mathbf{c}}^{\text{eff}}$ is the effective c-axis.

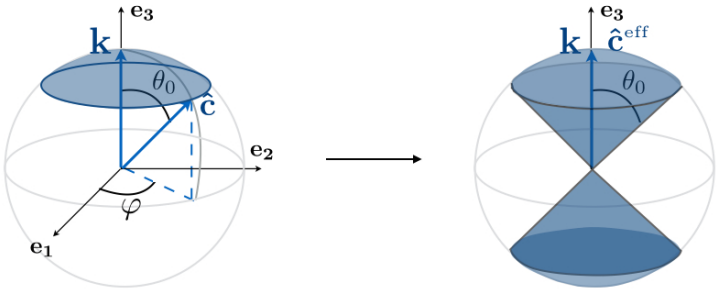

(a) (b)

Figure 3. Second configuration of the usual VTI clustered texture. (a) shows a typical c-axis $\hat{\mathbf{c}} = (\sin\theta\cos\varphi, \sin\theta\sin\varphi, \cos\theta)$ within one grain, θ varies in $[0, \theta_0]$ and φ varies randomly from grain to grain. (b) shows the resulting clustered, VTI, texture of the polycrystal at the macroscopic scale. $\hat{\mathbf{c}}^{\text{eff}}$ is the effective c-axis.

3.1 Wave propagation along the vertical axis in a polycrystal with VTI

We consider a wave propagating along the vertical axis, thus $\mathbf{k} = (0, 0, k)$, in a polycrystal with VTI, Figs. 2 and 3. The VTI structures provides that $\varphi \in [0,\ 2\pi]$ and is associated to a probability distribution independent of φ. Thus, the distribution of c-axes is given by probability distribution functions of the form

$$p(\theta, \varphi) = \frac{P_{\theta_0}(\theta)}{2\pi}, \quad \text{with} \int_0^{\pi/2} \mathrm{d}\theta \sin\theta P_{\theta_0}(\theta) = 1. \tag{13}$$

3.1.1 Velocities from the velocity averaging method

In this method, we first derive the velocities in a grain, and this is done without lack of generality for a wave propagating along $\mathbf{e}_3$. The Christoffel equation, Eq. (2) with $n_b = \delta_{b3}$ (same for n_c) simplifies to

$$\begin{vmatrix} \rho V^2 - C_{55} & -C_{45} & -C_{35} \\ -C_{45} & \rho V^2 - C_{44} & -C_{34} \\ -C_{35} & -C_{34} & \rho V^2 - C_{33} \end{vmatrix} = 0, \tag{14}$$

where the C_{IJ} is derived from c_{ijkl} in Eq. (6), for a c-axis given by Eq. (5)

$$\left\{\begin{array}{l} C_{33} = A\mathrm{s}\theta^4 + 2(2L+F)\mathrm{s}\theta^2\mathrm{c}\theta^2 + C\mathrm{c}\theta^4, \\ C_{44} = (A+C-2F)\mathrm{s}\theta^2\mathrm{c}\theta^2\mathrm{s}\varphi^2 + L\left[\mathrm{s}\varphi^2(\mathrm{c}\theta^2-\mathrm{s}\theta^2)^2 + \mathrm{c}\theta^2\mathrm{c}\varphi^2\right] + N\mathrm{s}\theta^2\mathrm{c}\varphi^2, \\ C_{55} = (A+C-2F)\mathrm{s}\theta^2\mathrm{c}\theta^2\mathrm{c}\varphi^2 + L\left[\mathrm{c}\varphi^2(\mathrm{c}\theta^2-\mathrm{s}\theta^2)^2 + \mathrm{c}\theta^2\mathrm{s}\varphi^2\right] + N\mathrm{s}\theta^2\mathrm{s}\varphi^2, \\ C_{34} = -\mathrm{s}\varphi\mathrm{s}\theta\mathrm{c}\theta\left[A\mathrm{s}\theta^2 - C\mathrm{c}\theta^2 + (2L+F)(1-2\mathrm{s}\theta^2)\right], \\ C_{35} = -\mathrm{c}\varphi\mathrm{s}\theta\mathrm{c}\theta\left[A\mathrm{s}\theta^2 - C\mathrm{c}\theta^2 + (2L+F)(1-2\mathrm{s}\theta^2)\right], \\ C_{45} = \mathrm{s}\varphi\mathrm{c}\varphi\mathrm{s}\theta^2\left[(A+C-2F)\mathrm{c}\theta^2 + L(1-4\mathrm{c}\theta^2) - N\right], \end{array}\right. \tag{15}$$

and we have used the notations $\mathrm{c}\varphi \equiv \cos\varphi$, $\mathrm{s}\varphi \equiv \sin\varphi$, $\mathrm{s}\theta \equiv \sin\theta$ and $\mathrm{c}\theta \equiv \cos\theta$. The determinant, Eq. (14), can be calculated and we get the roots ρV^2

$$\left\{\begin{array}{l} \rho V^2 = \left(L\mathrm{c}\theta^2 + N\mathrm{s}\theta^2\right), \\ (\rho V^2)^2 + \left(A\mathrm{s}\theta^2 + C\mathrm{c}\theta^2 + L\right)\rho V^2 - F^2\mathrm{s}\theta^2\mathrm{c}\theta^2 + AC\mathrm{s}\theta^2\mathrm{c}\theta^2 + AL\mathrm{s}\theta^4 + CL\mathrm{c}\theta^4 - 2FL\mathrm{s}\theta^2\mathrm{c}\theta^2 = 0. \end{array}\right. \tag{16}$$

The first root corresponds to a pure shear wave polarized in a direction perpendicular to both $\mathbf{k}$ and $\hat{\mathbf{c}}$, referred as the SH-wave. The two roots of the second equation are associated to the so-called quasi shear and quasi longitudinal waves, being coupled. The directions of polarization of the three waves are orthogonal (because the determinant is associated to a symmetric matrix) but the quasi longitudinal wave is in general not along $\mathbf{e}_3$ and the quasi shear wave is in general not in the $(\mathbf{e}_1, \mathbf{e}_2)$ plane. More explicitly, the three velocities read

$$\left\{\begin{array}{l} \rho V_{SH}^2 = L\mathrm{c}\theta^2 + N\mathrm{s}\theta^2, \\ \rho V_{SV}^2 = \dfrac{1}{2}\left[C + L + (A-C)\mathrm{s}\theta^2 - \sqrt{D}\right], \\ \rho V_{P}^2 = \dfrac{1}{2}\left[C + L + (A-C)\mathrm{s}\theta^2 + \sqrt{D}\right], \end{array}\right. \tag{17}$$

with $\quad D \equiv \left[A\mathrm{s}\theta^2 - C\mathrm{c}\theta^2\right]\left[A\mathrm{s}\theta^2 - C\mathrm{c}\theta^2 + 2L(\mathrm{c}\theta^2 - \mathrm{s}\theta^2)\right] + 4\mathrm{s}\theta^2\mathrm{c}\theta^2(F^2 + 2FL) + L^2.$

These are the expressions of the velocities in a single grain with a c-axis forming an angle θ with $\mathbf{k}$.

The second step in the velocity averaging method can be applied

$$\frac{1}{V^{\mathrm{av}}(\theta_0)} = \int_0^{2\pi} \mathrm{d}\varphi \int_0^{\pi/2} \mathrm{d}\theta\ \sin\theta\, p(\theta,\varphi) V^{-1}(\theta,\varphi) = \int_0^{\pi/2} \mathrm{d}\theta\ \sin\theta\, P_{\theta_0}(\theta) V^{-1}(\theta), \tag{18}$$

for $V = V_{SH}, V_{SV}, V_P$ taken from Eqs. (17). These last averages depend further on $P_{\theta_0}(\theta)$.

3.1.2 Velocities of the effective medium

With the probability function given by Eq. (13), the effective medium is characterized by a Voigt matrix

$$C_{IJ}^{\mathrm{eff}}(\theta_0) = \int_0^{2\pi} \frac{\mathrm{d}\varphi}{2\pi} \int_0^{\pi/2} \mathrm{d}\theta\ C_{IJ}(\theta,\varphi) \sin\theta\, P_{\theta_0}(\theta). \tag{19}$$

The Voigt matrix $C_{IJ}(\theta,\varphi)$ has 21 non-zero coefficients. Averaging $C_{IJ}(\theta,\varphi)$ over $\varphi \in [0,\, 2\pi]$ makes 15 of them to vanish, and the resulting Voigt matrix has a VTI symmetry, as expected, see Eqs. (A2)-(A3) in *Maurel et al.* (2015). The remaining integrations over θ depend on $P_{\theta_0}(\theta)$.

Next, the velocities of the elastic waves propagating along the $\mathbf{e}_3$ axis can be derived by solving the Christoffel equation, Eq. (2) with $C_{IJ} \to C_{IJ}^{\text{eff}}$. We get

$$\begin{vmatrix} \rho V^2 - C_{44}^{\text{eff}}(\theta_0) & 0 & 0 \\ 0 & \rho V^2 - C_{44}^{\text{eff}}(\theta_0) & 0 \\ 0 & 0 & \rho V^2 - C_{33}^{\text{eff}}(\theta_0) \end{vmatrix} = 0, \tag{20}$$

and we report below the intermediate results on C_{33} and C_{44} after φ-averaging, from Eq. (15),

$$\begin{cases} \langle C_{33} \rangle_\varphi(\theta) = A\mathrm{s}\theta^4 + 2(2L+F)\mathrm{s}\theta^2\mathrm{c}\theta^2 + C\mathrm{c}\theta^4, \\ \langle C_{44} \rangle_\varphi(\theta) = L\mathrm{c}\theta^2 + N\mathrm{s}\theta^2, \end{cases} \tag{21}$$

afterwards

$$C_{IJ}^{\text{eff}}(\theta_0) = \int \mathrm{d}\theta\, \langle C_{IJ} \rangle_\varphi(\theta) \sin\theta\, P_{\theta_0}(\theta). \tag{22}$$

The resulting effective velocities read

$$\begin{cases} V_P^{\text{eff}} = \sqrt{C_{33}^{\text{eff}}(\theta_0)/\rho}, \\ V_S^{\text{eff}} = \sqrt{C_{44}^{\text{eff}}(\theta_0)/\rho}. \end{cases} \tag{23}$$

The longitudinal wave has a velocity associated to the polarization along $\mathbf{e}_3$; more importantly for the present demonstration, the two transverse waves have polarizations in the $(\mathbf{e}_1, \mathbf{e}_2)$ plane and they are associated to the same velocity.

3.2 Examples of the velocity averaging method for polycrystals with VTI

3.2.1 Example 1: the VTI girdle with a single zenith angle θ_0

The first configuration is shown in Fig. 2. All the grains within the polycrystal have the same angle $\theta = \theta_0$ but different φ randomly distributed in $[0, 2\pi]$, whence

$$P_{\theta_0}(\theta) = \frac{\delta(\theta - \theta_0)}{\sin\theta_0}. \tag{24}$$

The velocities obtained from the velocity averaging method, Sec. 3.1.1, are obtained with V in Eqs. (17) and Eqs. (18) and (24), leading to

$$\begin{cases} V_{SH}^{\text{av}} = \sqrt{\dfrac{L\mathrm{c}\theta_0^2 + N\mathrm{s}\theta_0^2}{\rho}}, \\ V_{SV}^{\text{av}} = \sqrt{\dfrac{C + L + (A-C)\mathrm{s}\theta_0^2 - \sqrt{D}}{2\rho}}, \\ V_P^{\text{av}} = \sqrt{\dfrac{C + L + (A-C)\mathrm{s}\theta_0^2 + \sqrt{D}}{2\rho}}, \end{cases} \tag{25}$$

with $\quad D \equiv \left[A\mathrm{s}\theta_0^2 - C\mathrm{c}\theta_0^2\right]\left[A\mathrm{s}\theta_0^2 - C\mathrm{c}\theta_0^2 + 2L(\mathrm{c}\theta_0^2 - \mathrm{s}\theta_0^2)\right] + 4\mathrm{s}\theta_0^2\mathrm{c}\theta_0^2(F^2 + 2FL) + L^2.$

These velocities are reported in Figs. 4(a) (red curves) and they will be discussed later. We now derive the two shear and transverse velocities of the effective medium, Sec. 3.1.2, which are given by Eqs. (23) with $C_{IJ}^{\text{eff}}(\theta_0) = \int \mathrm{d}\theta \, \langle C_{IJ} \rangle_\varphi(\theta) \sin\theta \, P_{\theta_0}(\theta)$, and Eqs. (21) and (24). We get

$$\begin{cases} V_P^{\text{eff}} = \sqrt{\dfrac{1}{\rho}\left[A\mathrm{s}\theta_0^4 + 2(2L+F)\mathrm{s}\theta_0^2\mathrm{c}\theta_0^2 + C\mathrm{c}\theta_0^4\right]}, \\ V_S^{\text{eff}} = \sqrt{\dfrac{1}{2\rho}\left[(A+C-2F)\mathrm{s}\theta_0^2\mathrm{c}\theta_0^2 + L(4\mathrm{s}\theta_0^4 - 5\mathrm{s}\theta_0^2 + 2) + N\mathrm{s}\theta_0^2\right]}, \end{cases} \tag{26}$$

and these velocities are reported in black lines in Figs. 4(a).

3.2.2 Example 2: the VTI clustered texture with opening angle θ_0

This texture is shown in Fig. 3. It corresponds to

$$P_{\theta_0}(\theta) = \frac{H_{\theta_0}(\theta)}{1 - \cos\theta_0}, \tag{27}$$

where H_{θ_0} is the rectangular function, equals unity for $0 \leq \theta \leq \theta_0$, zero otherwise. The velocities $(V_{SH}^{\text{av}}, V_{SV}^{\text{av}}, V_P^{\text{av}})$ in the velocity averaging method, Sec. 3.1.1, cannot be calculated analytically in this case. The averages on θ in Eq. (18) are performed numerically (with Eqs. (17) and (27)), and they are shown in red lines in Fig. 4(b).

The velocities of the effective medium ($V_S^{\text{eff}}, V_P^{\text{eff}}$, Sec. 3.1.2) are calculated as previously, using Eqs. (21) to (23), with Eq. (27), and we get

$$\text{Cluster} \begin{cases} V_S^{\text{eff}} = \sqrt{\dfrac{(L+N)}{2\rho} + \dfrac{[2(A+C) - 4F - 3L - 5N]}{30\rho} X - \dfrac{[(A+C) - 2(2L+F)]}{10\rho} Y} \\ V_P^{\text{eff}} = \sqrt{\dfrac{A}{\rho} + \dfrac{[-7A + 3C + 4(2L+F)]}{15\rho} X + \dfrac{[A + C - 2(2L+F)]}{5\rho} Y} \end{cases} \tag{28}$$

with $X \equiv 1 + \cos\theta_0 + \cos^2\theta_0$ and $Y \equiv \cos^3\theta_0 + \cos^4\theta_0$. These results are shown in black lines in Fig. 4(b).

Let us now discuss Figs. 4. Black lines correspond to the velocities V_P^{eff} and V_S^{eff} and as previously said, a unique velocity V_S^{eff} is found from the effective medium theory, by construction. Red lines correspond to the velocities V_P^{av} and $(V_{SH}^{\text{av}}, V_{SV}^{\text{av}})$ from the velocity averaging method. The discrepancy is incidental for the longitudinal wave velocity and does not allow to discriminate between the two methods. The important result is that we find two distinct shear wave velocities using the velocity averaging method, which is unphysical in the present case.

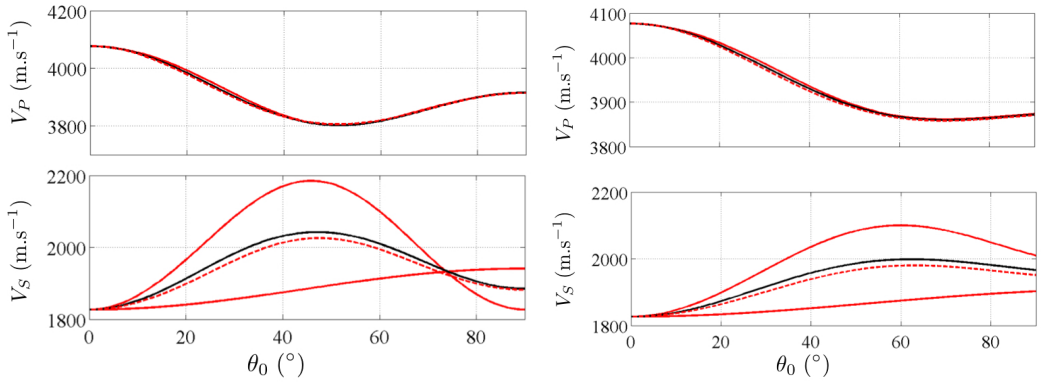

(a) (b)

Figure 4. Illustration of the inconsistency of the velocity averaging method for the two VTI textures shown in (a) Fig. 2 and (b) Fig. 3 The velocities V_P and V_S are reported as functions of θ_0, from the effective medium theory (black curves) and from the velocity averaging method (plain red lines). The dotted red lines show the shear wave velocity from Bennett's expression, close to the harmonic mean of the two unphysical shear wave velocities in plain red line.

4 Comment on Bennett's derivation of the velocities in the usual clustered texture

Bennett (1968) presented a calculation of the elastic velocities in the VTI cluster (Fig. 3), and he obtained a unique expression of the shear velocity. This result is in contradiction with the calculations performed in the previous section and reported in plain red lines in Fig. 4. To understand this discrepancy, we analyze the derivation proposed in *Bennett* (1968).

4.1 Bennett's calculations in *Bennett* (1968)

Bennett starts with the slownesses in a single crystal

$$S = 1/V,$$

given by

$$\begin{cases} S_1 = S_P \simeq a_1 - b_1 \cos 4\theta - c_1 \cos 2\theta, \\ S_2 = S_{SV} \simeq a_2 + b_2 \cos 4\theta, \\ S_3 = S_{SH} \simeq a_3 + b_3 \cos 2\theta, \end{cases} \tag{29}$$

where $(a_1, a_2, a_3, b_2, b_3)$ are constant for ice. The above expressions are close to the Thomsen approximations (*Thomsen*, 1986). They correspond to approximate expressions of the inverses of the velocities for the single crystals as given in Eqs. (17). In the above expressions, θ is the angle $(\mathbf{k}, \hat{\mathbf{c}})$ (Fig. 5(a)). Bennett used a different frame where neither $\mathbf{k}$ nor $\hat{\mathbf{c}}$ are along the direction $\mathbf{e}_3$. In this frame, he defined new multiple angles (Fig. 5(b)): $\sigma \equiv (\mathbf{k}, \mathbf{e}_3)$, $\theta = (\hat{\mathbf{c}}, \mathbf{e}_3)$ and $\hat{\theta} \equiv (\mathbf{k}, \hat{\mathbf{c}})$. An additional angle $\hat{\varphi}$, not represented in Fig. 5(a), between the planes $(\mathbf{k}, \mathbf{e}_3)$ and

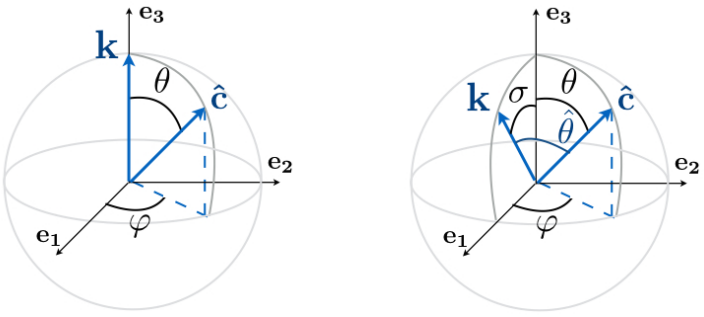

(a) (b)

Figure 5. (a) System of angles used in Bennett's calculations. $\hat{c}$ is given by (φ,θ) and $\mathbf{k}$ is given by σ, being otherwise in the $(\mathbf{e}_1,\mathbf{e}_3)$ plane. The extra angle $\hat{\theta}$ denotes the angle between $\mathbf{k}$ and $\hat{\mathbf{c}}$, thus $\cos\hat{\theta} = \sin\sigma\cos\varphi\sin\theta + \cos\sigma\cos\theta$. (b) Particular case of the Bennett configuration, for $\sigma = 0$; in this case, $\hat{\theta} = \theta$.

$(\mathbf{k},\hat{\mathbf{c}})$ is used. Next, an ensemble of relations between the different angles are derived, among which $\cos\hat{\theta} = \sin\sigma\cos\varphi\sin\theta + \cos\sigma\cos\theta$ and

$$\begin{cases} \sin^2\hat{\varphi} = \dfrac{\sin^2\varphi\sin^2\theta}{\sin^2\hat{\theta}}, \\ \cos^2\hat{\varphi} = \dfrac{(\cos\sigma\cos\varphi\sin\theta - \sin\sigma\cos\theta)^2}{\sin^2\hat{\theta}} \end{cases} \tag{30}$$

and these relations are correct, for instance if $\sigma = 0$, then $\hat{\theta} = \theta$ and $\hat{\varphi} = \varphi$, as expected. Next, it is said that the slowness of the wave depends on $\hat{\varphi}$ following

$$\begin{cases} S_P = S_1, \\ S_{SV} = S_2\cos^2\hat{\varphi} + S_3\sin^2\hat{\varphi}, \\ S_{SH} = S_2\sin^2\hat{\varphi} + S_3\cos^2\hat{\varphi}. \end{cases} \tag{31}$$

This is postulated by Bennett as being an intuitive approximation. Since $\hat{\varphi}$ can vary while $\hat{\theta}$ remains constant (see Eqs. (30)), the above equations pretend that the velocity of the shear waves depends on more than just $\hat{\theta}$, what Eq. (29) shows as incorrect. More explicitly, using $\sigma = 0$ (thus, $\hat{\theta} = \theta$, $\hat{\varphi} = \varphi$) in Eq. (31) and using Eqs. (29)-(30), we get

$$\begin{cases} S_{SV} = (a_2 + b_2) - 8b_2\cos^2\varphi\cos^2\theta\sin^2\theta - 2b_3\sin^2\varphi\sin^2\theta, \\ \\ S_{SH} = (a_2 + b_2) - 8b_2\sin^2\varphi\cos^2\theta\sin^2\theta - 2b_3\cos^2\varphi\sin^2\theta, \end{cases} \tag{32}$$

similarly to Eqs. (5-15) in *Bennett* (1968). These expressions for the velocities in a single crystal contain an unphysical dependence versus φ and they are not in agreement with the original expressions, Eqs (29), they derive from. The modification performed in Eqs. (31), when compared with the original expressions, consists in attributing symmetrical weights to both S_1 and S_2 in order to get an identical value for the two shear wave velocities, after velocity averaging. Bennett's results are reported in dotted red lines in Figs. 4. As expected, the shear wave velocity appears to be close to the

harmonic mean of the two unphysical velocities (resulting from the velocity averaging calculation). The velocity of the P-wave, being not modified by artificial weights, remains the same.

It is difficult to anticipate the consequences of such approach in the case of other textures, since the weights used to deduce the shear wave velocity in Eqs. (31) were chosen while anticipating a result expected after velocity averaging. The intuition that one can have for simple texture configuration may become hazardous when complex textures are dealt with.

5 Conclusions

In this paper, we have proposed a critical analysis of the velocity averaging method that has been used recently in the post treatment of the wave velocities deduced from borehole sonic logging measurements along ice cores. We have illustrated the error made in the fundamental assumption postulated at the basis of this method. This critical analysis is performed here in the case of simple VTI textures for which the error leads to an unphysical result, and thus allows for a clear demonstration. For VTI textures, Bennett circumvented this problem by postulating weighted forms of the shear wave velocities (*Bennett*, 1968). The method is clever but it requires to be able to anticipate good guesses for the selected weights, which may become difficult in the case of complex crystallographic textures.

The sonic logging measurements are sought as a proxy of the ice polycrystal anisotropy. Beyond the case of clustered VTI textures, complex textures could be characterized by such methods (or at least transitions between various textures with depth). On the one hand, the anisotropy of the ice single crystal is weak, and thus, the anisotropy of ice polycrystals is even weaker. But on the other hand, ice along boreholes is reasonably free of impurities when compared to most of the materials studied by similar sonic measurements. The recent sonic logging campaign performed at EPICA Dome C has revealed the feasibility of such measurements (*Gusmeroli et al.*, 2012). Nowadays, commercial loggers measure precisely the velocity. In parallel, the characterization of the physical properties of the ice single crystal and of the dependences of these properties with pressure and temperature reaches precisions of the order of a few percents. This increase in the precision renders the inverse problem accessible, from the measured velocities to the ice texture, but the inversion model still requires a high level of accuracy. With respect to this requirement, a rigorous model as the model based on the effective medium theory appears as a good candidate and should be favored.

References

Azuma, N., and Goto-Azuma, K. (1996). An anisotropic flow law for ice-sheet ice and its implications. Annals of Glaciology, 23, 202-208.

Bennett H.F. 1968 An investigation into velocity anisotropy through measurements of ultrasonic wave velocities in snow and ice cores from Green- land and Antarctica. Ph.D. thesis, University of Wisconsin, Madison, 1968.

Blankenship, D. D., Bentley, C. R., Rooney, S. T., and Alley, R. B. (1987). Till beneath Ice Stream B: 1. Properties derived from seismic travel times. Journal of Geophysical Research: Solid Earth (1978 - 2012), 92(B9), 8903-8911.

Diez, A., and Eisen, O. (2015). Seismic wave propagation in anisotropic ice-Part 1: Elasticity tensor and derived quantities from ice-core properties. The Cryosphere, 9(1), 367-384.

Diez, A., Eisen, O., Hofstede, C., Lambrecht, A., Mayer, C., Miller, H., Weikusat, I. (2015). Seismic wave propagation in anisotropic ice-Part 2: Effects of crystal anisotropy in geophysical data. The Cryosphere, 9(1), 385-398.

Diez, A., and Eisen, O. (2015). Seismic wave propagation in anisotropic ice-Part 1: Elasticity tensor and derived quantities from ice-core properties. The Cryosphere, 9(1), 367-384.

Gusmeroli, A., Pettit, E. C., Kennedy, J. H., and Ritz, C. (2012). The crystal fabric of ice from full?waveform borehole sonic logging. Journal of Geophysical Research: Earth Surface (2003-2012), 117(F3).

Keller JB. 1964 Stochastic Equations and Wave Propagation in Random Media. in *Proceedings of the 16th Symposium on Applied Mathematics* (AMS, New York, 1964) 145-179.

Karal Jr FC, Keller JB. 1964 Elastic, Electromagnetic and Other Waves in Random medium. *J. Math. Phys.* **5** 537-547.

Kohnen, H. (1974). The temperature dependence of seismic waves in ice. J. Glaciol, 13(67), 144-147.

Maurel, A., Lund, F., and Montagnat, M. (2015, May). Propagation of elastic waves through textured polycrystals: application to ice. In Proceedings of the Royal Society of London A: Mathematical, Physical and Engineering Sciences (Vol. 471, No. 2177, p. 20140988). The Royal Society.

Middya, T. R., Paul, M., and Basu, A. N. (1986). Multiple scattering theoretical and computer simulated dynamic model approaches to effective elastic properties of randomly disordered composites. Journal of applied physics, 59(7), 2376-2381.

Thomsen GW. 1986 Weak elastic anisotropy. *Geophysics* **15** 1954-1966.

Thorsteinsson T. 1990 Textures and fabrics in bottom silty ice from the Dye 3 ice core. University of Copenhagen, MS thesis.

Voigt W. 1928 Lehrbuch der Kristallphysik, reprint of the 1st edn. Leipzig: Teubner.

Vélez, J. A., Tsoflias, G. P., Black, R. A., Van der Veen, C. J. and Anandakrishnan, S. (2016). Distribution of preferred ice crystal orientation determined from seismic anisotropy: Evidence from Jakobshavn Isbræand the North Greenland Eemian Ice Drilling facility, Greenland. Geophysics, 81(1), WA111-WA118.